scientific reports

OPEN

Anthropogenic activities accelerate LULC conversion and only a sustainable development scenario is optimal for agro-pastoral ecotone development

Jing Jin[1,2,3✉], Zilong Liao[1,2,3], Tiejun Liu[1,2,3], Mingxin Wang[1,2,3], Jing Zhang[1,3], Xinjian Zhang[3] & Yining Fan[4]

Despite the ecological and socioeconomic importance of agro-pastoral ecotones, changes in land use and land cover (LULC) and their driving mechanisms are not comprehensively understood. In this study, a systematic framework for LULC assessment covering comprehensive timeframes was constructed for the Tabu watershed. Results demonstrated that a new process of LULC changes began in 1998, with a significant increase in farmland and decrease in grassland. The increase in dynamic degrees and structural variation coefficients indicated intensive and frequent changes in LULC. Conversion ratios between grassland and farmland exceeded 95%, and construction land encroached upon grassland. Grassland changes were driven mainly by natural factors based on the random forest regression, as well as changes in farmland and construction land. The influence of anthropogenic drivers on LULC became significant. Under the sustainable development scenario, the increase in grassland with a high fractional vegetation cover in 2034 was the most significant, the area of bare land decreased, the area of construction land steadily increased, and the reduction in farmland area was under control. Under this scenario, both socioeconomic development and ecosystem stability can be achieved. This study provides insights into regional land dynamics and provides systematic guidance for sustainable land management.

Keywords Tabu watershed, Timescale, New process, Random forest regression, Markov–PLUS model, Sustainable development

Land use is a critical manifestation of human activities[1], and humans obtain food and other materials for living and production by utilizing and exploiting land resources. Notably, land use and land cover (LULC) changes affect the global climate, water circulation, carbon cycle and biodiversity[2,3]. To achieve sustainable development and ecological resilience, comprehending the intricacies of LULC is imperative[4].

The beginning of LULC research was tracked back to Agenda 21, which was proposed by the United Nations in 1992, and early research focused mainly on the classification and spatial mapping of land use types (LUTs)[5]. Since the beginning of the 21st century, more attention has been given to the spatiotemporal changes in LULC and the associated driving mechanisms, with administrative units with significant LULC changes used as the study areas. Zheng et al.[6] found that stringent land management was conducive for controlling LULC conversion by analyzing the spatiotemporal changes in LULC over the 1990–2015 period. Meng and Si[7] noted that the urban lands in Yangzhou city quickly expanded from 2005 to 2018, which was caused mainly by increases in fixed–asset investment, the urban population and farmland. Land use conflicts between agriculture, construction, and ecology are more serious than they were before, and these conflicts could be mitigated by dividing spatial control zones[8,9]. Dammag et al.[10] analyzed the spatiotemporal characteristics of LULC in 1990, 2005 and 2020 in

[1]Yinshanbeilu Grassland Eco-Hydrology National Observation and Research Station, China Institute of Water Resources and Hydropower Research (MWR), Beijing 100038, China. [2]Collaborative Innovation Center for Grassland Ecological Security (Jointly Supported by the Ministry of Education of China and Inner Mongolia Autonomous Region), Hohhot 010021, China. [3]Institute of Pastoral Hydraulic Research, MWR, Hohhot 010021, China. [4]Hebei University of Engineering, Handan 056000, China. ✉email: jinjingmwr@163.com

Ibb city, Yemen, and emphasized the importance of planning and managing sustainable land use via a cellular automate (CA)–Markov model. On the basis of the analysis of LULC changes in the agro-pastoral ecotone of Gansu Province from 2000 to 2020 via the Geo-detector, Li and Yan reported that socioeconomic factors had a strong explanatory power for LULC changes[11]. Through future scenario simulations, policies related to farmland protection and ecological priorities can improve land use efficiency and sustainable development[4,8]. With the advancement of the LULC Change Project and Global Land Project, various disciplines (ecology, socioeconomics, geography and others) have been integrated with LULC research, which has contributed to the sustained interest in studying LULC[10–13]. Therefore, LULC datasets have been taken as the basis for studying ecosystem services in recent years[3,14], and it has been demonstrated that LULC changes play significant roles in hydrological balance[15], carbon storage[16], habitat quality[17], etc.

Research on LULC has widely developed in various fields, such as spatiotemporal evolution, driving mechanisms, and ecosystem services[2,10,16]. However, these studies are mainly based on a specific temporal span or predefined time intervals, such as five-year or ten-year periods[11,18–20]. Nevertheless, both natural and human factors play a role in influencing LULC changes[2,11,21]. Among them, human factors possess a certain degree of subjectivity and randomness. Therefore, human activities may be guided by different development goals during different periods, leading to corresponding different changes in LULC[2,22]. Regrettably, previous studies have often overlooked this crucial aspect. Overall analysis or the analysis based on artificially defined periods may not accurately reflect the phased characteristics of LULC changes, affecting the quantitative assessment of the driving mechanisms of LULC changes and even posing a risk to simulation accuracy.

Technological advancements in remote sensing provide powerful tools for LULC research[2]. The Environmental Systems Research Institute (ESRI) of the United States, Google, the National Geomatics Center of China and some famous universities (such as Tsinghua University and Wuhan University) offer high-precision LULC datasets with diverse resolutions[20,23]. Leveraging these datasets significantly facilitates the study of LULC simulations. The main methods for simulating LULC changes include the Markov model, CA model, future land use simulation (FLUS) model and patch–generating land use Simulation (PLUS) model. Each method has advantages and disadvantages. The Markov model can quantitatively predict future change trends, but it has difficulty reflecting spatial changes[24]. Owing to the lack of a module to regulate the transformation of cellular states, the CA model is confined to a special LUT[25]. The FLUS model has high execution efficiency because it couples the system dynamics, CA and neural network models together, but it falls short in clearly reflecting the spatial differences among different LUTs[20]. In the PLUS model, the land expansion analysis strategy (LEAS) is combined with the CA model based on multitype random patch seeds (CARS), thereby achieving higher simulation accuracy[14,26,27]. Improving the reliability of LULC simulation is still a hot but challenging topic of future research[14,16,34], and the integration of multiple methods will be conducive to achieving scientific simulation results.

The evaluation of an object's evolution and its relevant policies and measures are always based on a temporal framework. Spatiotemporal analysis of LULC changes is helpful for understanding LUT changes, gauging the degree of utilization, and determining the critical milestones in LULC evolution[2,4]. Unraveling the driving mechanism is conducive to identifying favorable and unfavorable factors, thereby guiding humans to strategically capitalize on beneficial factors and mitigate the impact of detrimental factors when utilizing land resources[7,11]. According to LULC simulations, the accessibility of LULC development goals under different scenarios and the effectiveness of policies and implementation measures can be scientifically evaluated[13,24,28]. Given the circumstances of land use conflicts and sustainable development, there is an urgent need for a comprehensive framework that incorporates the aforementioned aspects. This framework enables systematic analysis from change assessment to driver identification, and to scenario simulation, which will greatly promote in-depth LULC theoretical research toward practical application.

Within agro-pastoral ecotones, both agriculture and stock farming are well developed, resulting in various LUTs that undergo frequent conversions[5]. Compared with urban and agricultural areas, these ecotones present distinctive characteristics across ecological, economic and sociocultural domains[5,11]. Using these areas to conduct LULC research is beneficial for revealing the evolutionary characteristics of both artificial and natural landscapes, as well as the relationships between them. The Tabu watershed, an agro-pastoral ecotone undergoing frequent LULC changes, plays an important role in protecting the ecological health of northern China. Its multifaceted significance renders it an ideal site for LULC research. However, there is currently a gap in LULC research.

To fill these gaps, this study aims to establish a systematic framework for studying LULC evolution covering comprehensive timeframes, and the Tabu watershed was taken as a case study. The research objectives were to (1) analyze LULC changes from spatial and temporal perspectives, (2) identify new LULC process and quantitatively analyze the driving factors, and (3) simulate future LULC changes under three scenarios by using the Markov–PLUS model. This study is expected to deepen the understanding of LULC dynamics over time and provide scientific basis for policymakers and land managers to develop land use conservation strategies and sustainable development initiatives for these critical ecosystems.

Materials and methods
Study area
The study area is nestled in the northern Yinshan Mountain, Inner Mongolia, China (41°2′–42°51′N, 110°33′–112°10′ E). It covers an area of 10,370 km^2 (Fig. 1), and grassland and farmland cover more than 90% of the area. The terrain gently slopes from south to north, with the elevation lowering from 2167 to 948 m. Along with the terrain, the landforms transition from hills, mountains, and high plains to alluvial–proluvial plains. The Tabu River, one of the four major inland rivers in Inner Mongolia flowing from south to north, has transitioned from a perennial river to an intermittent river over the past two decades. Human settlements and cultivated land are distributed mainly in the southern area along the riverbank, and grassland is widely distributed in the
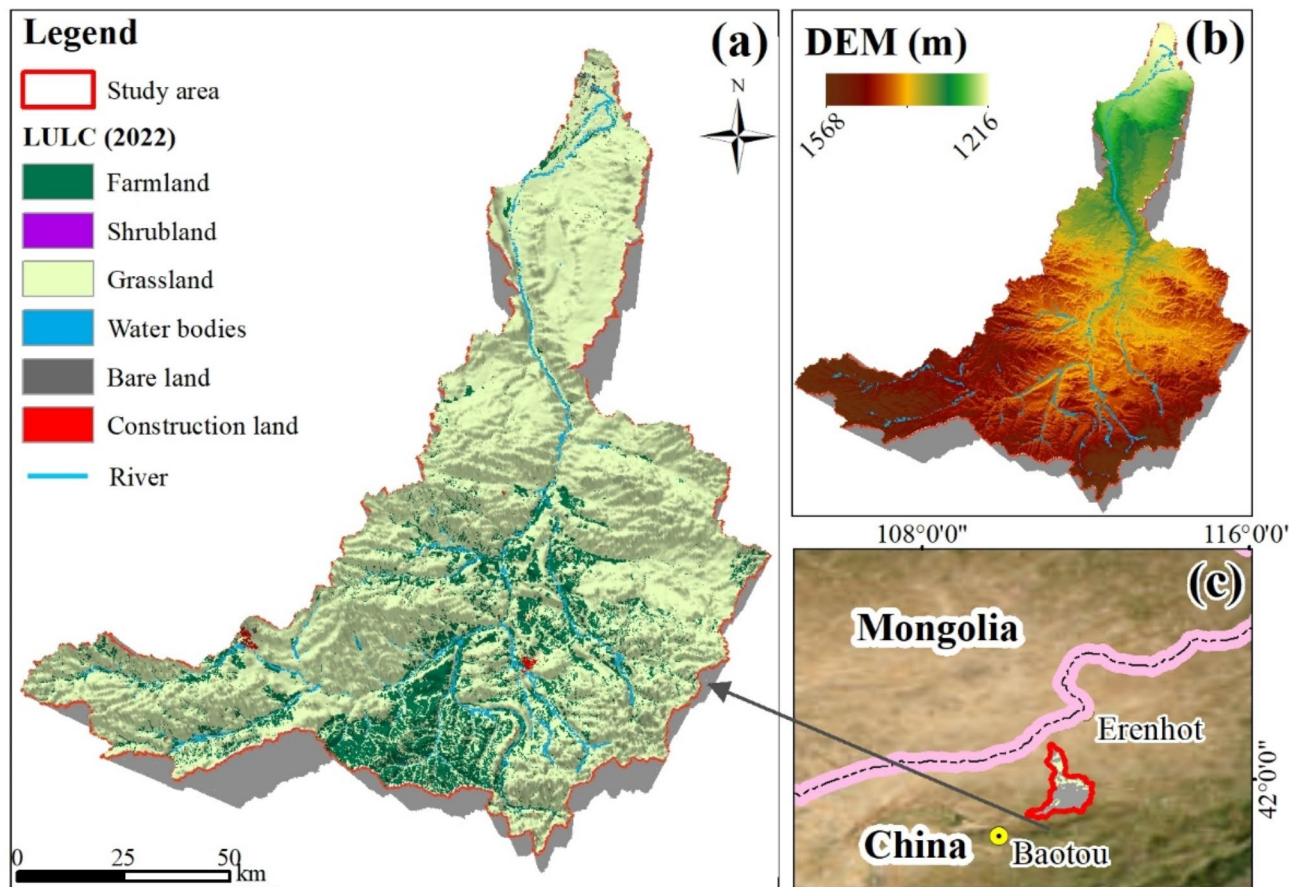
Fig. 1. LULC in 2022 (**a**), digital elevation model (DEM) (**b**) and location of the study area (**c**).

central and northern areas. Grassland, known as the Earth's skin, plays a vital role as an ecologically protective screen and in the pastoral development sector in northern China. Characterized by a typical arid to semiarid continental monsoon climate, the region experiences an average annual temperature of 3.36 °C and a mean annual precipitation of 311.2 mm, with most rainfall occurring from July to September.

Data collection and preprocessing

LULC data with a spatial resolution of 30 m were obtained from the annual China Land Cover Dataset (CLCD) from 1985 to 2022. The overall accuracy of the dataset reaches 79.31%, which is higher than those of other datasets, such as MCA12Q1, EASCCI_LC, and GlobalLand30[23]. The LUTs within the study area were reclassified into six types: farmland, shrubland, grassland, water bodies, construction land, and bare land. Considering spatial variability, comprehensiveness, and accessibility, fourteen factors were selected as potential drivers of LULC evolution, reflecting both natural and anthropogenic influences. Details of the data sources are listed in Table 1.

Owing to the requirements of the PLUS model, all datasets necessitated preprocessing to ensure the uniformity of the coordinate system, area size, and spatial resolution. With the aid of the defined projection tool, the coordinate systems of all the data were unified to WGS_1984_Albers. The spatial resolutions of these datasets were subsequently adjusted to match those of the LULC dataset (30 m × 30 m) via the resampling tool. Finally, all the data were processed to retain the same size of 7095 rows by 4884 columns via the mask extraction tool. When identifying the driving factors in a certain period, only one set of driving data is needed. Taking the average values of sequential data is a common method[9,26,27]. For example, the average precipitation was calculated on the basis of the precipitation database from 1998 to 2010 via the raster calculator, and the average data was input into the random forest regression (RFR) module to analyze its driving contribution. The data for gross domestic product (GDP) and population were not continuous, but the datasets at five-year intervals (2000, 2005, 2010, 2015 and 2020) were accessible. Similarly, the averages of these data of the years 2000, 2005 and 2010 were calculated to analyze their driving contributions.

Grassland constitutes more than 80% of the study area, and external factors have different impacts on the fractional vegetation cover (FVC) of grassland[29]. To more clearly elucidate the driving mechanism and LULC simulation under future scenarios, grassland was subdivided into three types based on the FVC: low–FVC grassland (L–FVC, ≤ 0.2), medium–FVC grassland (M-FVC, 0.2–0.5), and high–FVC grassland (H–FVC, ≥ 0.5).

Data		Original resolution/ proportion scale	Data source and preprocessing
LULC data (1985–2022)		30 m×30 m	China Land Cover Dataset (CLCD) of Wuhan University (https://essd.copernicus.org/articles/13/3907/2021/)
Enhanced Vegetation Index (EVI, 1998–2022)		250 m×250 m	Earth data (https://search.earthdata.nasa.gov/). The data were converted to TIFF format by using MODIS Reprojection Tools.
FVC (1998–2022)		250 m×250 m	FVC was calculated by using the dimidiate pixel model based on EVI[29].
Driver	GDP (2000, 2005, 2010, 2015 and 2020)	1 km×1 km	Resource and environment science and data center (https://www.resdc.cn/Default.aspx)
	Population (2000, 2005, 2010, 2015 and 2020)		
	Precipitation (1998–2022)		National Earth System Science Data Center, National Science & Technology Infrastructure of China (http://www.geodata.cn)
	Temperature (1998–2022)		
	Evaporation (1998–2022)		
	Soil texture	1:1000000	Harmonized World Soil Database version (HWSD) (https://www.fao.org/soils-portal/soil-survey/soil-maps-and-databases/ harmonized-world-soil-database-v12)
	Elevation	30 m×30 m	Geographic data cloud (https://www.gscloud.cn/home)
	Slope	30 m×30 m	By using the Slope tools, the slope data was obtained based on the elevation data.
	Distance from river (DR)	1:1000000	National catalogue service for geographic information (https://www.webmap.cn/main.do? method=index). These distances were subsequently calculated by the Euclidean distance function based on the raster data.
	Distance from residential site (DRS)		
	Distance from highway (DH)		
	Distance from first grade road (DFR)		
	Distance from secondary road (DSR)		
	Distance from tertiary road (DTR)		

Table 1. Details regarding the dataset of LULC and drivers.

Methodology

In this study, a comprehensive framework of LULC analysis was developed based on the LULC maps of the agro-pastoral ecotone from 1985 to 2022. First, the spatial and temporal characteristics of LULC were investigated via geostatistical analysis, the dynamic degree and the land use conversion matrix over a long timescale[30]. Second, the key year was identified based on the Mann–Kendall (M–K) mutation test and the accumulative anomaly method[31], and it was considered as the beginning of a new LULC process. Third, the contributions of the driving factors to LULC changes were quantitatively evaluated by employing the RFR[32,33]. Finally, the LULC changes under future scenarios were simulated based on the Markov–PLUS model[14,24].

(1) Dynamic degrees of LULC and structural variation coefficient (C_t).

The dynamic degrees (D_s and D_c) can reflect the changes in the quantity of LUTs[11,19]. D_s is the single dynamic degree which is used to reflect the changing rate and amplitude of a special LUT during a certain period. D_c is the comprehensive dynamic degree and can reflect the general changes in all LUTs by considering the conversion among different LUTs. The equations are as follows:

$$D_s = \frac{U_b - U_a}{U_a} \times \frac{1}{T} \times 100\% \tag{1}$$

$$D_c = \left(\frac{\sum_{i,j=1}^{n} \Delta U_{ij}}{2 \sum_{i=1}^{n} U_i} \right) \times \frac{1}{T} \times 100\% \tag{2}$$

where U_a and U_b denote the quantities of a specific LUT at the beginning and end of the period, respectively; U_i denotes the quantity of a certain LUT; ΔU_{ij} is the absolute value of the conversion of LUT i into LUT j during a given period ($i \neq j$); and T is the study duration from year a to year b. If the value of D_s is greater than 0, the area of the LUT increases; otherwise, the area of the LUT decreases. The higher the values of D_s and D_c are, the more obvious the changes in the specific LUT and all LUTs.

The C_t value is used to measure the LULC variations between two time points in the study area; the higher the C_t value is, the greater the difference is. C_t is based on the Euclidean distance and can be calculated by the following equation[11]:

$$C_t = \sqrt{\sum_{i=1}^{n} (P_{bi} - P_{ai})^2} \tag{3}$$

where i denotes LUT i; t denotes the study period; and P_{bi} and $P_{a.i.}$ denote the proportions of LUT i at the beginning and end of the study period, respectively. The C_t values can be classified into three levels: minor variation ($0 < C_t \leq 0.25$), moderate variation ($0.25 < C_t \leq 0.50$), and significant variation ($C_t > 0.5$)[6].

(2) RFR.

Principal component analysis (PCA), multiple linear regression and analytic hierarchy process (AHP) are widely used in analyzing driving factors. PCA achieves dimensionality reduction by extracting the principal components, which may lead to ambiguous definitions of the principal components[34]. Multiple linear regression is simple and easy to implement, but its result is confined by the linear assumption and influenced by the

multicollinearity issue[24]. The AHP has poor applicability when dealing with many factors[35]. RFR is an ensemble learning algorithm based on decision trees which can handle large amounts of high-dimensional data[9,26,32]. This method has a strong ability to handle nonlinear relationships and can avoid the excessive influence of outliers on driving analysis[33]. Moreover, RFR can perform feature selection and anomaly detection[26]. Based on the above advantages, RFR was employed to analyze the contributions of driving factors to LULC changes quantitatively.

The PLUS model has an RFR module to obtain the contribution ratios of factors driving LULC changes and the development potential of LUTs under the driving mechanisms. Referring to studies proposed by Liang et al.[26], who developed the PLUS model, the number of regression trees was set to 50, the sampling rate was set to 0.1 to obtain more precise accuracy, and the mTry value was set to 14 which is the number of driving factors. The smaller the root mean square error (RMSE) is, the higher the accuracy is[36]. The RMSE results were all less than 0.09, so the analysis results based on RFR were considered to be reliable.

(3) Markov-PLUS model.

The PLUS model integrates the LEAS and CARS modules to improve simulation accuracy[9]. The LEAS module can extract the expansion parts of every LUT between two-time nodes and then obtain the development probabilities of the LUTs based on the quantitative analysis of the driving mechanism. The CARS module is used to achieve scenario simulation based on the development probabilities and LULC conversion matrices, which effectively improves the operating stability. This model overcomes several problems, such as the complexity of traditional conversion rules and the lack of a period concept when analyzing LULC patterns. Owing to these advantages, the PLUS model has been widely used in simulating LULC changes in recent years[9,14,27].

The PLUS model is based on the following two assumptions[26,27]: (1) an inertia assumption of historical development, that is, the future LULC will unfold in accordance with the historical development patterns, and (2) an assumption of the stability of the driving mechanism, indicating that the influences of the driving factors on the current LULC changes remained relatively constant over time. However, the development needs of various LUTs differ under different scenarios, so it is necessary to preset the quantities and scales of LUTs on the basis of future development goals. The Markov model provides an effective way to predict LUT changes by using the matrices of the conversion probabilities according to the LULC datasets[8,10]. The integration of the Markov and PLUS models effectively improves the simulation accuracy both in terms of quantity and spatial distribution[9,24]. The primary framework of the Markov-PLUS model is shown in Fig. 2.

The overall accuracy (OA), kappa coefficient, and figure of merit (FoM) were used to validate the precision and accuracy of the simulation results of the Markov-PLUS model. The OA and kappa coefficient were employed to assess the simulation accuracy from an overall perspective, while the FoM was used to objectively evaluate changes in the number of cells[27]. Generally, a kappa coefficient greater than 0.6 and an FoM greater than 0.2 indicate satisfactory simulation consistency[8,24].

Scenario simulation settings

Scientific LULC simulations and predictions not only help to elucidate development trends and changes but also enable the verification of whether the current socioeconomic development model can effectively guide the rational utilization of future land resources and enhance regional ecosystem functions[19,20]. The future LULC in the target year (2034) was simulated under different scenarios based on historical LULC change trends (1998–2022) and future developmental goals.

(1) Natural development scenario (NDS).

Under this scenario, the historical development potential, LULC expansion capabilities, neighborhood weights, and other parameters are applied to the model[26], and the Markov model was employed to predict the quantities of LUTs in 2034. The other scenarios are based on the NDS.

(2) Urban development scenario (UDS).

In accordance with the social development strategy, the plan of Never Crossing the Red Line for the Protection of Cultivated Land was adopted and for sustainability purposes, the society and economy in the study area would continue to steadily develop, and full consideration would be given to farmland protection. In this scenario, construction land would continuously increase, and the areas of permanent and high-quality farmlands would remain stable[28]. Thus, under the UDS, the conversion probabilities of shrubland, grassland, and bare land to construction land increase by 30%, whereas the permanent and high-quality farmlands are not converted to other LUTs due to farmland protection policies.

(3) Sustainable development scenario (SDS).

Sustainable development, which considers both socioeconomic development and ecological protection, is significant for national survival and development. According to the political tasks for constructing an ecological barrier in northern China, a series of measures (afforestation, grassland restoration, and ecological water replenishment for contracting lakes and rivers) should be implemented to improve the ecological environment. Under the SDS, the conversion probabilities of shrubland and grassland to construction land and farmland decrease by 40%, the conversion probabilities of lower FVC grassland to higher FVC grassland increase by 40%, and the conversion probabilities of bare land to shrubland and grassland increase by 20%. To ensure agricultural development within the agro-pastoral ecotone and food security, it was imperative to constrain the rapid decline in farmland under the SDS compared with that under the NDS. As a result, not only were the areas of permanent and high-quality farmlands constrained to be stable[19], but the conversion probabilities of farmland to other LUTs were also assumed to decrease by 40%. Water bodies are restored, and the areas of water bodies serve as constraints in the Markov–PLUS model, limiting their conversion into other LUTs.

The conversion matrix was constructed for the three scenarios to illustrate the conversion relationships among different LUTs. In the matrix (Table 2), "1" indicates that a particular LUT could be converted into another, whereas "0" signifies that such a conversion was not possible between the two LUTs. Based on previous studies[20,37], the possibility of construction land being converted into other LUTs is relatively low with
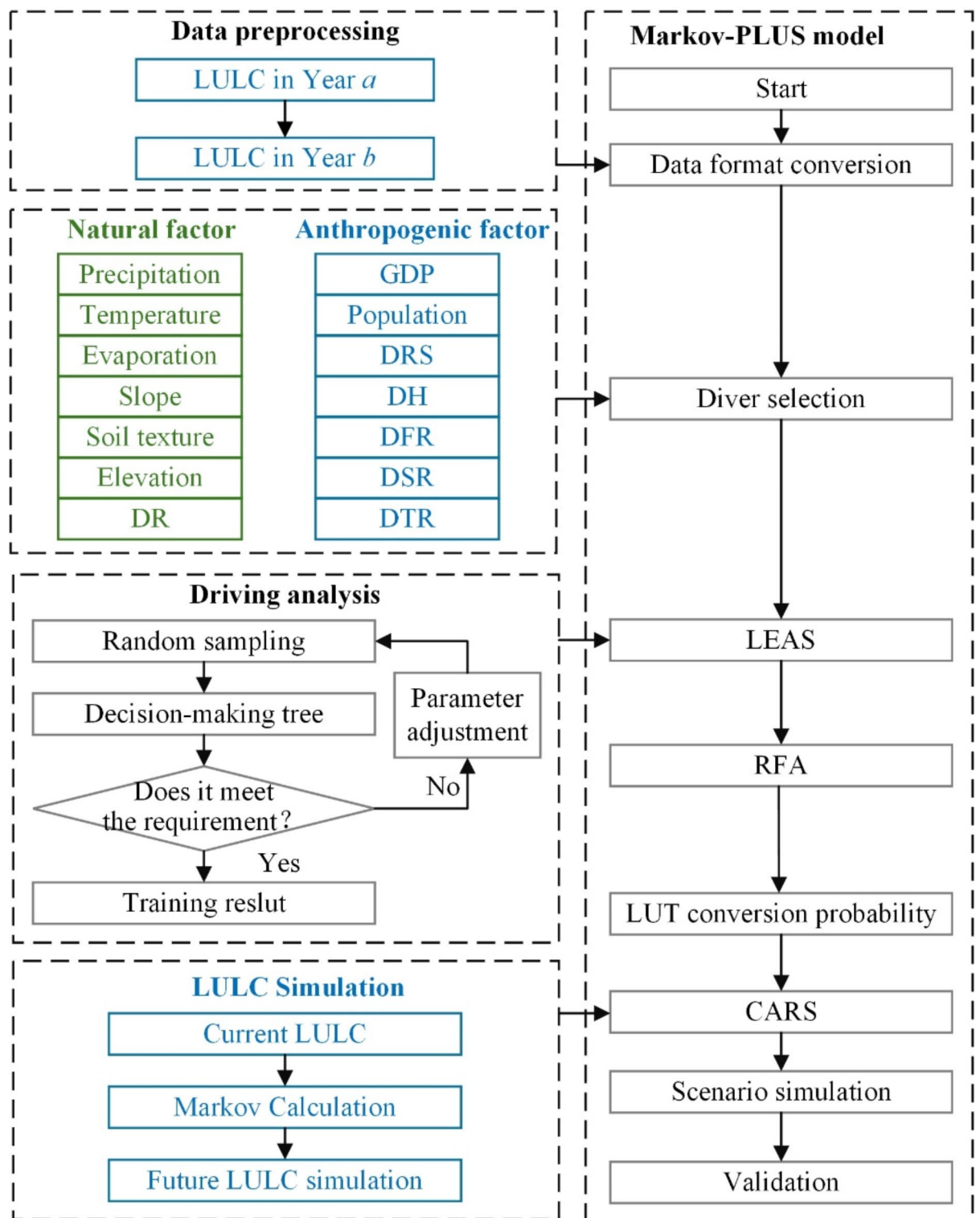
Fig. 2. Framework of the Markov–PLUS model.

Future scenario	LULC	Farmland	Shrubland	L–FVC grassland	M–FVC grassland	H–FVC grassland	Waterbodies	Bare land	Construction land
NDS	Farmland	1	1	1	1	1	1	1	1
	Shrubland	1	1	1	1	1	1	1	1
	L–FVC grassland	1	1	1	1	1	1	1	1
	M–FVC grassland	1	1	1	1	1	1	1	1
	H–FVC grassland	1	1	1	1	1	1	1	1
	Water bodies	1	1	1	1	1	1	1	1
	Bare land	1	1	1	1	1	1	1	1
	Construction land	0	0	0	0	0	0	0	1
UDS	Farmland	1	1	1	1	1	1	1	1
	Shrubland	1	1	1	1	1	1	1	1
	L–FVC grassland	1	1	1	1	1	1	1	1
	M–FVC grassland	1	1	1	1	1	1	1	1
	H–FVC grassland	1	1	1	1	1	1	1	1
	Water bodies	1	1	1	1	1	1	1	1
	Bare land	1	1	1	1	1	1	1	1
	Construction land	0	0	0	0	0	0	0	1
SDS	Farmland	1	1	1	1	1	1	1	1
	Shrubland	1	1	1	1	1	1	1	1
	L–FVC grassland	1	1	1	1	1	1	1	1
	M–FVC grassland	1	1	1	1	1	1	1	1
	H–FVC grassland	1	1	1	1	1	1	1	1
	Water bodies	0	0	0	0	0	1	0	0
	Bare land	1	0	0	0	0	1	1	1
	Construction land	0	0	0	0	0	0	0	1

Table 2. Conversion matrix settings for the UDS, UDS and SDS scenarios.
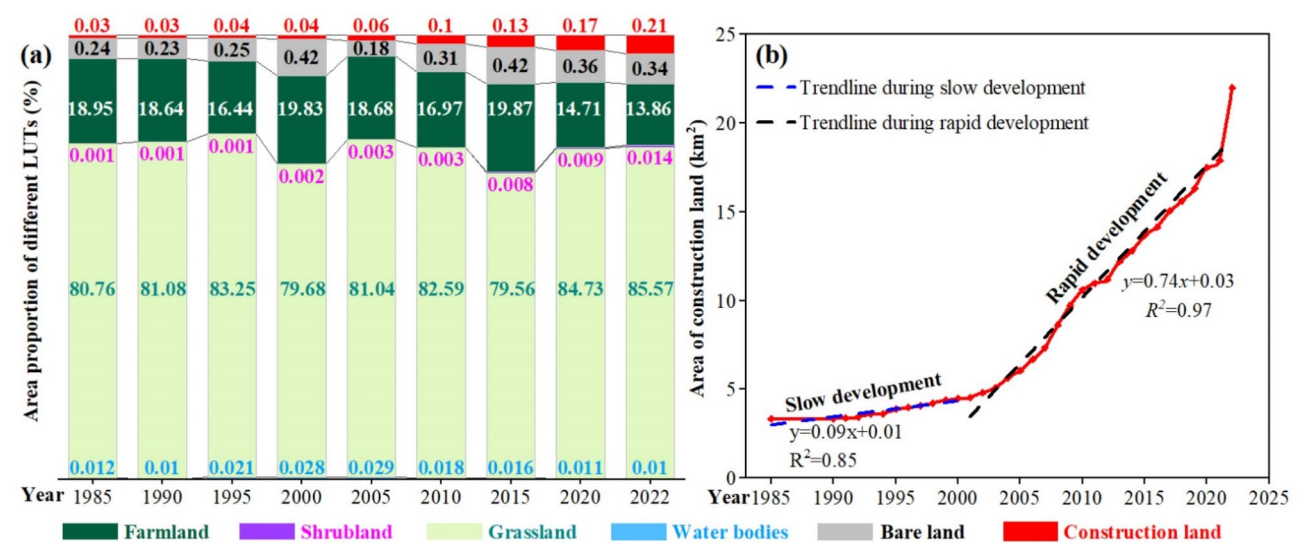

Fig. 3. Changes in LULC (**a**) and expansion of construction land (**b**) from 1985–2022.

socioeconomic development. Thus, the conversion coefficient for construction land was set to 0. The conversion coefficients of the other LUTs were set based on the development goals of the different scenarios[8].

Results
Changes in LULC from 1985 to 2022
Grassland covered more than 80% of the study area and were extensively distributed in the central and northern areas (Figs. 1a and 3a). Farmland accounted for approximately 13.86–19.87% of the total area and was concentrated mainly in the south. The area of construction land was relatively small, urban areas were clustered

in the southeast, while rural areas were dispersedly distributed across the study area. Shrubland was sparsely distributed and accounted for less than 0.02% of the total area. Water resources were scarce, and water bodies accounted for only approximately 0.01% of the total area, with surface water existing in the form of seasonal rivers and small ponds. Bare land covered less than 0.4% of the total area and was primarily concentrated in the northern part where precipitation was less than 150 mm and the deserted grassland with low FVC were widely distributed.

From a temporal perspective (Fig. 3a), the grassland area exhibited an increasing trend spanning from 1985 to 2022, which contrasted with the decreasing trend in the farmland area. This indicated a reciprocal relationship between grassland and farmland. There were notable declines in grassland during the 1995–2020 and 2010–2015 periods. Grassland loss was caused mainly by urban expansion, agricultural activities (e.g. land cultivation), and afforestation initiatives. Water bodies initially increased, peaked in 2005, and then decreased. Shrubland exhibited a significant increase, expanding from 0.12 km² in 1985 to 11.63 km² in 2022. The area of bare land progressively increased overall, with the area in 2022 increasing by 42% compared with that in 1985. The area of construction land has consistently increased from 1985 to 2022, especially over the past two decades, indicating the intensive expansion of urban and rural areas (Fig. 3b).

According to the D_s values (Table 3), the changes in farmland, shrubland, and bare land were relatively notable compared with those in the other LUTs. The dynamic changes in grassland were relatively small, but the changes in its area were significant. For instance, the D_s value of shrubland was 27.85%, and there was only an annual increase in area of 2.57 km² during the period from 2020 to 2022. Conversely, grassland exhibited a D_s value of only 0.49%, with an average annual expansion area of 43.38 km² in the 2020–2022 period. The D_c and C_t values were relatively low from 1985 to 1990. Both the D_c and C_t values subsequently increased, reaching peaks from both 1995–2000 and 2015–2020, indicating significant changes in LUTs during these periods.

New LULC process

The study area is a typical agro-pastoral ecotone, with grassland representing the natural landscape and farmland representing the artificial landscape. Therefore, the changes in the two LUTs were further analyzed to identify new LULC process. According to the M–K mutation test and the accumulative anomaly method, there was a notable upward trend in farmland and a notable downward trend in grassland since 1998 (Fig. 4). In the early 1990 s, China implemented a series of ecological protection projects, such as the returning of farmland to forest[37]. As a result, the area of farmland in that phase significantly decreased, whereas the area of grassland increased. By the end of the 1990 s, policies related to food security, including agricultural taxes reduction and exemption, as well as land consolidation promotion, had been implemented, leading to an increase in farmland and a decrease in grassland. Since 2017, the area of farmland began to decrease, whereas that of grassland increased. This occurred because the regional government carried out strict irrigation water management and advanced the Three-North Shelter Forest Program. These measures forced some farmland without irrigation to be converted to meadow for water conservation to some extent[38]. However, the mutation point (2017) identified by the M–K mutation test did not coincide with the inflection point (2021) of the cumulative anomaly curve. If the year 2017 was taken as a time node, the study period only spanned five years from 2017 to 2022, which was too short to proceed with a comprehensive study, and the simulation based on the short timescale may led to large errors[25]. Therefore, considering 2017 as the key year was inappropriate, let al.one holding the same prospect for 2021. As shown in Table 3, the values of D_s, D_c and C_t during the 1995–2000 period significantly increased compared with those during the 1990–1995 period, indicating that significant changes in LULC began. Thus, 1998 was a mutation time for LULC evolution, indicating a new process of land utilization.

LULC changes are influenced by the development goals of human society to a certain extent[9]. Since 1998, people have pursued rapid socioeconomic development, resulting in significant expansion of construction land and farmland. Accompanying the awareness of environmental protection, efforts have been made to strike a balance between socioeconomic development and ecological health, leading to the recovery of ecological landscapes. Therefore, with distinctive characteristics of human societal development at different stages, LULC also exhibited phased transformations, as depicted in Fig. 4. Identifying new process is beneficial for studying LULC evolution. Moreover, when the evolutionary characteristics of new process are applied in future

| Period | D_s (%) | | | | | | D_c | C_t |
	Farmlands	Shrubland	Grassland	Water bodies	Bare land	Construction land		
1985–1990	−0.34	−2.21	+ 0.08	−2.85	−0.26	+ 0.18	0.06	0.0045
1990–1995	−2.35	+ 4.79	+ 0.53	+ 22.28	+ 1.50	+ 3.11	0.44	0.0308
1995–2000	+ 4.12	+ 17.73	−0.86	+ 6.92	+ 13.11	+ 3.05	0.71	0.0492
2000–2005	−1.15	+ 4.73	+ 0.34	+ 0.13	−11.24	+ 6.97	0.27	0.0179
2005–2010	−1.84	−0.74	+ 0.38	−7.41	+ 14.42	+ 15.20	0.35	0.0232
2010–2015	+ 3.42	+ 34.42	−0.74	−2.12	+ 6.62	+ 5.79	0.61	0.0420
2015–2020	−5.19	+ 2.16	+ 1.30	−6.91	−2.47	+ 5.55	1.04	0.0731
2020–2022	−2.90	+ 27.85	+ 0.49	−4.45	−4.05	+ 12.87	0.44	0.0120

Table 3. Dynamic degree (D_s and D_c) and C_t values of LULC. With respect to D_s, "+" denotes an increase in area, whereas "−" denotes a decrease in area. The units of D_s and D_c were %.
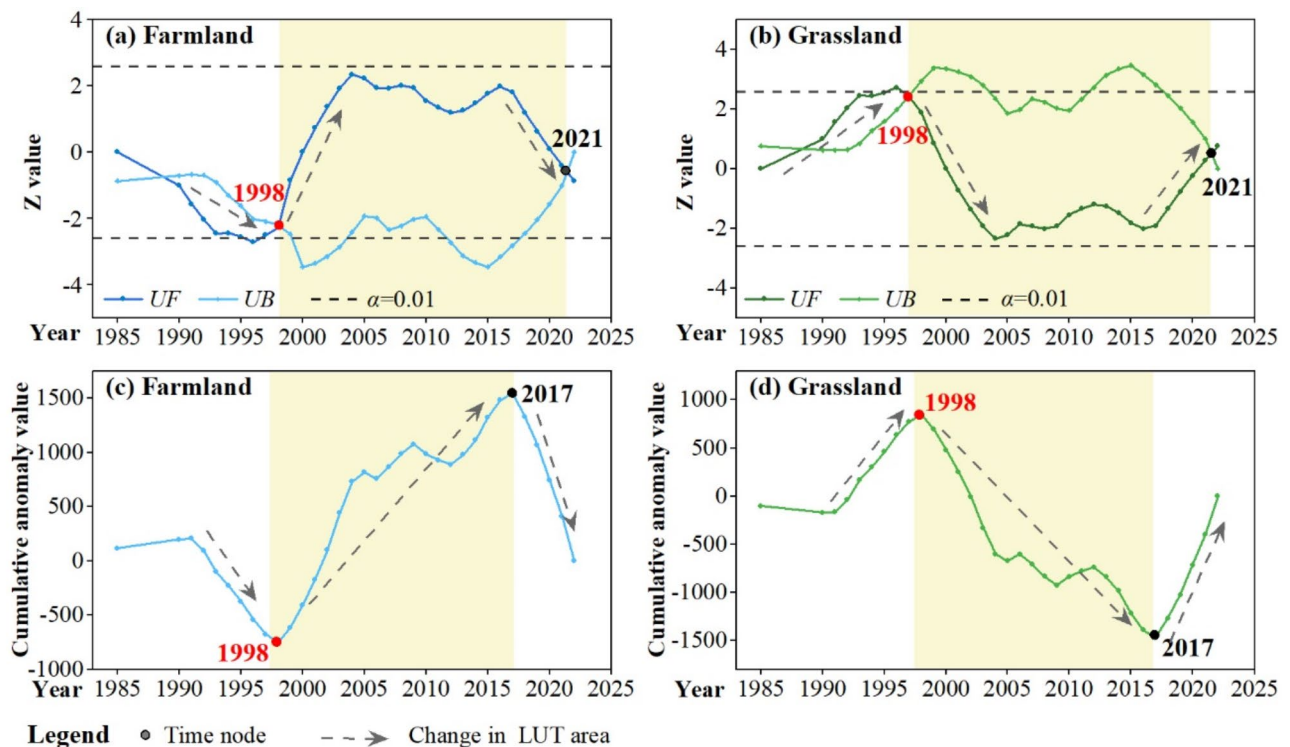
Fig. 4. *UF* and *UB* curves of farmland (**a**) and grassland (**b**) based on the M-K mutation test; and the accumulative anomaly curves of farmland (**c**) and grassland (**d**). The intersection points of the *UF* and *UK* curves and the inflection points of the accumulative anomaly curves were considered as the time nodes, which indicated that significant changes occurred. The changes in the LUT area were judged on the basis of the *UF* and accumulative anomaly curves.

simulations, the results could more accurately align with recent development trends. For these reasons, the following analysis of LULC was focused on the 1998–2022 period.

Land conversion

According to Fig. 5, it was demonstrated that the conversions between grassland and farmland were relatively significant. From 1998 to 2010, 514.35 km² of other LUTs were converted into farmland, of which 513.85 km² was derived from grassland, with a contribution of 99.90%. From 2010 to 2022, 238.91 km² of other LUTs were converted into farmland, with grassland accounting for 238.82 km², with a contribution of 99.96%. During the 1998–2010 period, 549.75 km² of other LUTs were converted into grassland, and the contribution of farmland reached 95.58%. From 2010 to 2022, 574.31 km² of other LUTs were converted into grassland, with farmland accounting for 97.51% of this conversion. Construction land increased by 6.38 km² and 11.38 km² during the 1998–2010 and 2010–2022 periods, respectively. The increased area of construction land was converted mainly from grassland, contributing up to 84.42% and 85.79% in the two periods, respectively. There were frequent conversions among farmland, grassland, water bodies and bare land (Table 4), and the conversion contributions of grassland to bare land were greater than 95%. Compared with that in 2010, the area of bare land in 2022 increased by 2.33 km², which was caused mainly by a large amount of grassland being converted into bare land. These finding indicate that the grassland has degraded to a certain extent. The increase in shrubland was attributed primarily to the conversion of grassland, along with a small portion of conversion from farmland.

Identification of the drivers of LULC changes

Fourteen factors were selected as potential drivers of LULC changes, seven of which were natural and seven of which were anthropogenic. According to the RFR results (Fig. 6), all the RMSE values were less than 0.09, and even the RMSE of shrubland was only 0.002. These low RMSE values indicate that the results are reliable and can be used for in-depth analysis of the driving mechanism[36].

As shown in Fig. 6, population and elevation were the primary drivers of farmland, and evaporation and DH were the main drivers of shrubland. The distribution of L–FVC grassland was strongly driven by elevation and distances from roads (DH and DFR), while the distributions of M–FVC and H–FVC grassland were driven mainly by precipitation, temperature and elevation. The most significant driver of water bodies changed from slope to precipitation from 1998 to 2022, and the contributions of the two drivers were 74.31% and 38.22%, respectively. Slope, temperature and elevation played significant roles in the conversion of bare land. The expansion of construction land was significantly driven by DFR and slope.
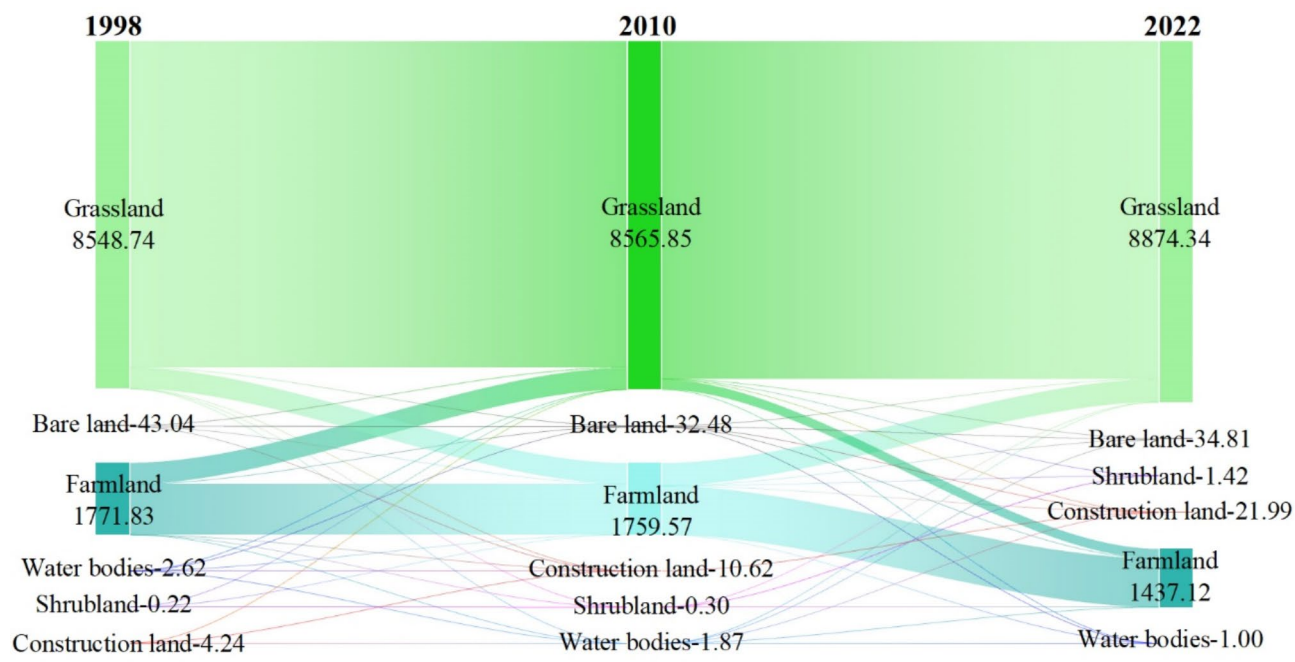
Fig. 5. Sankey diagram of the conversions among different LUTs from 1998 to 2010 and up to 2022. The numerical values following the LUTs represented the area of the LUTs at the specific time, expressed in km².

Periods	Other LUTs converted into bare land			Bare land converted into other LUTs		
	Direction: ——>		Conversion area	Direction: ——>		Conversion area
1998–2010	Farmland		0.24		Farmland	0.01
	Grassland	Bare land	12.71	Bare land	Grassland	23.48
	Water bodies		0.07		Construction land	0.10
2010–2022	Farmland		0.03		Farmland	0.04
	Grassland	Bare land	16.05	Bare land	Grassland	13.44
	Water bodies		0.25		Construction land	0.50

Table 4. Conversion between other LUTs and bare land. The LUTs that are not listed in the table indicate that no conversion occurred between them and bare land. The unit of the conversion area was km².

A comparison of the driving contributions during the two periods revealed that anthropogenic drivers, such as distances from roads (DH, DFR, DSR and DTR), contributed more to the changes in farmland, shrubland, grassland and water bodies in the 2010–2022 period than they did in the 1998–2010 period. In particular, the contribution of DH to shrubland increased the most significantly, and the contribution in the later period increased by 13 times compared with that in the previous period. For bare land, the contribution of slope increased to 28.51% and became to the most significant driver from 2010 to 2022, while the contribution of population also increased, and the contributions of other anthropogenic drivers decreased. The primary driver of construction land changed from DFR with a 22.48% contributing rate to slope with a contributing rate of 19.01%. This occurred because steeper slopes amplified the cost of land development and imposed greater restrictions on construction land expansion[28]. The influences of GDP, population and distances from roads (DH, DFR and DSR) on construction land decreased in the later period. On the contrary, natural factors such as rainfall, temperature, evaporation and the DEM increased. Given that construction land is an artificial LUT, these changes in the contributions of its drivers signaled alterations in policies and an increased emphasis by humans on creating livable environments.

Scenario simulations

Comparing the simulated LULC result for 2022 with the ground truth data, the simulation accuracy of the Markov–PLUS model was high, with the OA of 0.84, a kappa coefficient of 0.71, and an FoM of 0.48. This indicated that the model was favorably configured and produced reliable simulations[24]. Thus, the LULC simulations under the three scenarios (NDS, UDS and SDS) were achieved and are shown in Fig. 7; Table 5.

Under the NDS (Fig. 6a; Table 5), the areas of farmland and L–FVC grassland in 2034 decreased by 166.33 km² and 62.93 km², respectively, compared with those in 2022, with corresponding reduction ratios of −11.57% and − 0.95%, respectively. The areas of shrubland, M–FVC grassland, H–FVC grassland, water bodies, bare land
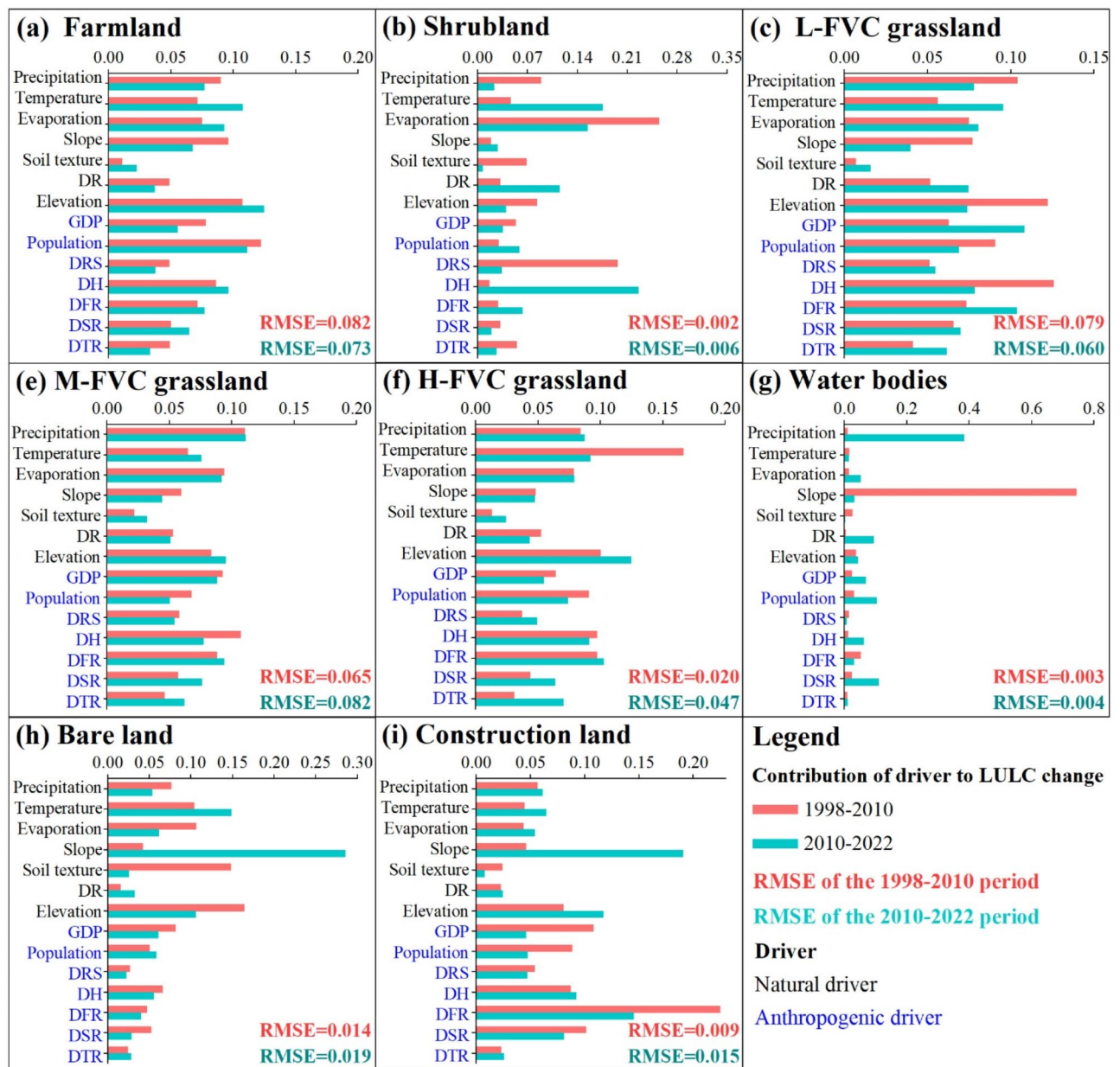
Fig. 6. Contributions of the natural and anthropogenic drivers to LUTs during the periods 1998–2010 and 2010–2022.

and construction land all exhibited increases compared with those in 2022, with the most significant increase being observed in H–FVC grassland. The LULC changes under the NDS were similar to those during the 2010–2022 period.

Under the UDS (Fig. 6b; Table 5), more attention was given to construction land, and its area markedly increased by 23.97% compared with that in 2022, and it was primarily concentrated near the town. The increasing ratios of M–FVC and H–FVC grassland were lower than those under NDS, whereas the increasing ratio of bare land increased from 3.69 to 9.11%. Considering of the protection of permanent and high-quality farmland, the reduction ratio of farmland decreased from 11.57% under the NDS to 9.50% under the UDS.

Under the SDS (Fig. 6c; Table 5), the increase in H–FVC grassland in 2034 was the most significant, with an increasing ratio of +49.85% compared with that in 2022. The areas of other natural LUTs (M–FVC grassland, water bodies and shrubland) all showed increasing trends. The area of bare land decreased by 1.20% compared with that in 2022, which was unattainable under the other scenarios. L–FVC grassland experienced a notable reduction of 146.66 km^2, which was converted into M–FVC grassland. In other words, the degree of desertification was under control and showed signs of improvement under the SDS. The area of construction land increased by 15.68%, which was intermediate between those under the NDS and UDS. These findings indicate that the study area could achieve stable development. Under this scenario, more measures of farmland
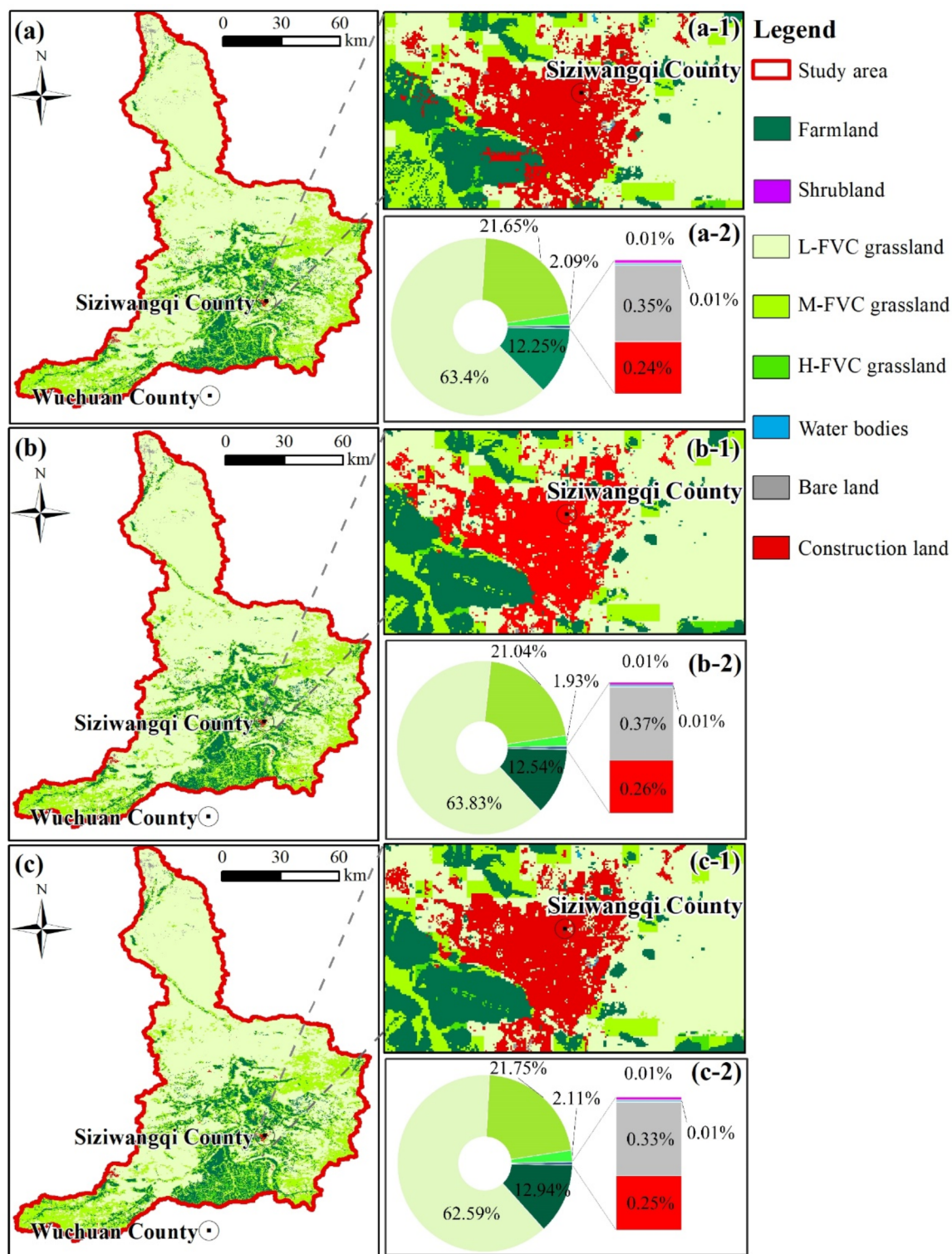
Fig. 7. Simulated LULC results for 2034 under the different scenarios: NDS (**a**), UDS (**b**), and SDS (**c**). The spatial distributions of LULC near the town under the three scenarios are shown in **a-1**, **b-1** and **c-1**, while the respective proportions of each LUT are shown in **a-2**, **b-2** and **c-2**.

Changes in area (2022–2034)		Farmland	Shrubland	L–FVC grassland	M–FVC grassland	H–FVC grassland	Water bodies	Bare land	Construction land
NDS	km²	−166.33	+ 0.12	−62.93	+ 154.71	+ 70.46	+ 0.0153	+ 1.28	+ 2.68
	%	−11.57	+ 8.22	−0.95	+ 7.40	+ 48.17	+ 1.54	+ 3.69	+ 12.17
UDS	km²	−136.54	−0.15	−17.93	+ 91.90	+ 54.26	+ 0.0144	+ 3.17	+ 5.27
	%	−9.50	−10.87	−0.27	+ 4.40	+ 37.09	+ 1.45	+ 9.11	+ 23.97
EDS	km²	−94.81	+ 0.02	−146.66	+ 165.52	+ 72.89	+ 0.01	−0.42	+ 3.45
	%	−6.60	+ 1.71	−2.21	+ 7.92	+ 49.83	+ 1.18	−1.20	+ 15.68

Table 5. Changes in the areas of the different LUTs under the different scenarios. The unit of the changing area is km²; the relative change rate compared with that in 2022 is expressed in %; "+" denotes an increase in area; and "−" denotes a decrease in area.

protection were formulated, so the reduction ratio of farmland decreased to 6.60%. Compared with the ratios under the historical trend and the NDS and UDS scenarios, the significant declining trend of farmland was effectively controlled under the SDS.

Discussion

In the process of LULC evolution in the study area, notable conversion occurred between grassland and farmland, and the expansion of construction land encroached upon grassland. These findings demonstrated an inherent competitive relationship among various LUTs in the agro-pastoral ecotone[5,11]. Land use conflicts are inevitable in the development of human society, and maintaining a balance in the reasonable distribution of farmlands and construction lands while ensuring the normal ecological functions of grassland ecology poses a significant challenge for future land management strategies[8,28].

Under the NDS, the changes in LULC aligned with the historical trends from 2010 to 2022, which were manifested by a substantial decrease in farmland, a significant increase in grassland, and a continuous increase in construction land. The significant increase in grassland area was attributed mainly to the implementation of ecological protection measures, such as strict water resource management and the Three–North Shelter Forest Program[39], especially after 2017. The restrictions on irrigation water, to some extent, indirectly led to the conversion of some non-irrigated farmland into meadows for water conservation purposes. The continuous substantial reduction in farmland may pose a threat to food security. Under the UDS, urban development and population increases were accompanied by a rising demand for food. Although the areas of permanent and high-quality farmland were formulated be stable, the rapid decline in farmland remained uncontrolled, which was inconsistent with the rapid development of construction land. What was worse, the increase rates of M–FVC and H–FVC grassland slowed, and the area of bare land increased. All of these might impede regional development.

Under the SDS, the conversion probabilities from bare land and lower FVC grassland to higher FVC grassland increased from the perspective of ecological protection, while the conversion probabilities from farmland to other LUTs decreased from the perspectives of agricultural and pastoral development as well as food security. In fact, many ecological production measures such as afforestation, grassland restoration, eco-water replenishment, and the control of livestock quantities have been carried out in the study area[39–41]. Meanwhile, the regional government actively encourages the development of bare land and saline–alkali land for plants, and prohibits construction land from encroaching on permanent and high-quality farmland[42]. These measures indicate that people have recognized the importance of balancing ecological protection and socioeconomic development. The SDS represents the optimal scenario for the development of the agro-pastoral ecotone. The abovementioned measures should be implemented in the long term. Additionally, in-depth studies on the carry capacity of grassland, farmland and water resources should be integrated into LULC planning. Under this scenario, the win–win goal of socioeconomic development and ecosystem stability can be achieved.

Farmland and construction land are typical anthropogenic landscapes, yet they are also influenced by natural factors, such as precipitation and slope. This finding fully reflects that humans adhere to natural laws during the process of land utilization[43]. As human development progresses, anthropogenic drivers, such as distances from roads (DH, DFR, DSR and DTR), contribute more to changes in farmland, shrubland, grassland and water bodies. This finding confirmed that land use was the result of various natural and anthropogenic factors[44], which was consistent with studies by Dammag[10] and Shi[20] et al. It also reaffirmed that sustainable development is based on complying with natural laws and the orderly development of human activities.

Compared with previous studies, this study presented several advantages: (1) the new process of LULC was identified to analyze the recent spatiotemporal evolution characteristics of LUTs, which was conducive to improving the reliability and accuracy of LULC simulation; (2) the integration of the Markov–PLUS model effectively improved the simulation accuracy both in terms of quantity and spatial distribution; and (3) under the UDS and SDS, the incorporation of farmland protection policies was considered, which made the scenarios setting more realistic and practical, and the simulated LULC was more precise and provided more insightful guidance for land use and management.

However, certain shortcomings were also present. (1) The resolutions of the raster data were inconsistent; for example, the LULC resolution was 30 m ×30 m, but the original resolutions of the precipitation, GDP and population data were relatively low (1 km×1 km), and such low resolutions might obscure some information

that affects the analysis of relationships and driving mechanisms. (2) Scenarios were formulated by artificially defining the development goals and conversion probabilities. Various measures, such as afforestation, grassland restoration, and the exploitation of bare land and saline–alkali land are being implemented. However, owing to the uncontrollability of natural factors and the implementation effect, there may be a deviation between the simulation results and real LULC changes. (3) Land use conflict is inevitable in the agro–pastoral ecotone, and the carrying capacities of construction land, farmland and grassland areas should be further studied and integrated into LULC simulations.

Conclusion

In this study, a systematic framework for LULC assessment covering comprehensive timeframes was constructed within an agro-pastoral ecotone. 1998 was identified as the beginning of a new LULC process, with a significant increase in farmland and a significant decrease in grassland. There was notable conversion between farmland and grassland, with conversion rates exceeding 95%, and construction land primarily encroached on grassland. Compared with that in 2010, the area of bare land in 2022 increased by 2.33 km^2, which was caused mainly by a large amount of grassland being converted into bare land. Grassland was influenced primarily by precipitation, temperature and other natural factors. Although farmland and construction land were anthropogenic landscapes, they are also influenced by natural factors, such as precipitation and slope. As human development progressed, anthropogenic drivers contributed more to the changes in farmland, shrubland, grassland and water bodies. According to the analysis of the LULC simulations under the three scenarios, the SDS was optimal for LULC development in the agro-pastoral ecotone. Under this scenario, the increase in H–FVC grassland in 2034 was the most significant with an increasing ratio of + 49.85% compared with that in 2022. The area of bare land decreased by 1.20% compared with that in 2022, which was unattainable under the other scenarios. The reduction ratio of farmland decreased to 6.60% and the area of construction land continuously increased, and these changes were conducive to the socioeconomic development and food security. The SDS would achieve a win–win goal of socioeconomic development and ecosystem stability, which could provide meaningful guidance for efficient land utilization.

Limited by the inconsistency in the data resolution and subjectivity of human activities, the simulations may deviate from reality to some extent. Further research should focus on the acquisition of high-precision data and the carrying capacities of LUTs to more accurately simulate LULC changes under future scenarios.

Data availability

Data publicly available in a repository.(1) LULC datasets can be obtained from Earth System Science Data (https://essd.copernicus.org/articles/13/3907/2021/. (2) The data of GDP, population are available as open data via Resource and environment science and data center (https://www.resdc.cn/Default.aspx). (3) The data of precipitation, temperature and evaporation data were available as open data via National Earth System Science Data Center, National Science & Technology Infrastructure of China (http://www.geodata.cn). (4) The soil texture data can be obtained from Harmonized World Soil Database version (HWSD) (https://www.fao.org/soils-portal/soil-survey/soil-maps-and-databases/harmonized-world-soil-database-v12). (5) The elevation data are available in Geographic data cloud (https://www.gscloud.cn/home), and the slope data can be obtained by processing the elevation data with the Slope tool. (7) The raster data of first grade road, secondary road, tertiary road, highway, residential site and river are obtained from National catalogue service for geographic information (https://www.webmap.cn/main.do?method=index). These distances (DFR, DSR, DTR, DH, DRS, DR) are subsequently calculated by the Euclidean distance function based on the raster data. (8) The Enhanced Vegetation Index (EVI) dataset is obtained from Earth data (https://search.earthdata.nasa.gov/), and then the fractional vegetation cover (FVC) data are calculated by using the dimidiate pixel model based on EVI.

References

1. Mooney, H. A., Duraiappah, A. & Larigauderie, A. Evolution of natural and social science interactions in global change research programs. *Proc. Natl. Acad. Sci.* **110**, 3665–3672. https://doi.org/10.1073/pnas.1107484110 (2013).
2. Du, Z. R. et al. Land use/cover and land degradation across the Eurasian steppe: dynamics, patterns and driving factors. *Sci. Total Environ.* **909**, 168593. https://doi.org/10.1016/j.scitotenv.2023.168593 (2024).
3. Li, Y. G. et al. The role of land use change in affecting ecosystem services and the ecological security pattern of the Hexi regions, Northwest China. *Sci. Total Environ.* **855**, 158940. https://doi.org/10.1016/j. scito tenv.2022.158940 (2023).
4. Feng, Y. W., Zhang, W. Z., Yu, J. H. & Zhuo, R. R. Optimization of land-use pattern based on suitability and trade-offs between land development and protection: a case study of the Hohhot-Baotou-Ordos (HBO) area in inner Mongolia, China. *J. Clean. Prod.* **466**, 142796. https://doi.org/10.1016/j.jclepro.2024.142796 (2024).
5. Zhai, Y. J., Zhang, Y. H., Jiang, Q. G. & Liu, R. Spatia-temporal evolution pattern of production-living-ecological space in agro-pastoral ecotone of Western Jilin Province. *J. Jilin Univ. (Earth Sci. Edition)*. **52**, 1016–1026. https://doi.org/10.13278/icnkijjuese.20210185 (2022).
6. Zheng, Y. T., Zhao, S., Huang, J. Y. & Lv, A. F. Analysis of the Spatiotemporal pattern and mechanism of land use mixture: evidence from China's County data. *Land* **10**, 370–370. https://doi.org/10.3390/land10040370 (2021).
7. Meng, L. & Si, W. T. The driving mechanism of urban land expansion from 2005 to 2018: the case of Yangzhou, China. *Int. J. Res. Public. Health*. **19**, 15821. https://doi.org/10.3390/ijerph192315821 (2022).
8. Chen, L. T. & Cai, H. S. Study on land use conflict identification and territorial Spatial zoning control in Rao river basin, Jiangxi Province. *China Ecol. Indic.* **145**, 109594. https://doi.org/10.1016/J.ECOLIND.2022.109594 (2022).
9. Li, H. Z. Multi-scenario simulation of production-living ecological space in the Poyang lake area based on remote sensing and RF-Markov-PLUS Model. (2023). https://doi.org/10.27178/d.cnki.gjxsu.2023.000550

10. Dammag, A. Q., Dai, J., Basema, G. C., Latif, Z. H. & Q. D. & Predicting spatio-temporal land use/land cover changes and their drivers forces based on a cellular automated Markov model in Ibb City, Yemen. *Geocarto Int.* **38**, 2268059. https://doi.org/10.1080/10106049.2023.2210532 (2023).

11. Li, W. X. & Yan, Z. G. Analysis of Spatiotemporal evolution of land use and its driving mechanism in the agro-pastoral ecotone of Gansu Province using geodetector. *Arid Zone Res.* **41**, 590–602. https://doi.org/10.13866/j.azr.2024.04.06 (2024).

12. Yang, S. A. et al. Assessing land–use changes and carbon storage: a case study of the Jialing river basin, China. *Sci. Rep.* **14**, 15984. https://doi.org/10.1038/s41598-024-66742-2 (2024).

13. Yang, J. X. et al. Simulating urban expansion using cellular automata model with spatiotemporally explicit representation of urban demand. *Landscape Urban Plan.* 231, 104640. (2022). https://doi.org/10.1016/J.LANDURBPLAN. 104640 (2023).

14. Tang, H. et al. Ecosystem service valuation and multi-scenario simulation in the ebinur lake basin using a coupled GMOP-PLUS model. *Sci. Rep.* **14**, 5071. https://doi.org/10.1038/s41598-024-55763-6 (2024).

15. Hassan, K. et al. Quantitative analysis of land use land cover (LULC) changes on the hydrological behavior of the Jhelum river basin: North-west Himalayas, Kashmir. *Water Conserv. Sci. En.* **9**, 78. https://doi.org/10.1007/S41101-024-00311-6 (2024).

16. Paramesha, V. et al. Evaluating land use and climate change effects on soil organic carbon. A simulation study in coconut and pineapple systems in West Coast India. *Catena* **248**, 108587. https://doi.org/10.1016/j.catena.2024.108587 (2025).

17. Zhang, G. J. & Quan, L. Impact of habitat quality changes on regional thermal environment: a case study in Anhui Province, China. *Sustainability* **16**, 8560. https://doi.org/10.3390/su16198560 (2024).

18. Feng, Y. J. et al. Spatially-explicit modeling and intensity analysis of China's land use change 2000–2050. *J. Environ. Manage.* **263**, 110407. https://doi.org/10.1016/j.jenvman.2020.110407 (2020).

19. Jia, T. C. & Hu, X. W. Spatiotemporal dynamic evolution characteristics of land use in China's' two screens and three belts' ecological barrier areas from 1985 to 2020. *Res. Soil. Water Conserv.* **31**, 348–363. https://doi.org/10.13869/j.cnki.rswc.2024.04.038 (2024).

20. Shi, F. F. Land use/land cover change, driving forces, and prediction in the Huangshui River Basin, Qinghai. https://link.cnki.net/doi/10.27778/d.cnki (2024). https://doi.org/10.27778/d.cnki.gqhzy.2024.000012

21. Cui, X. F. et al. Spatial-temporal responses of ecosystem services to land use transformation driven by rapid urbanization: a case study of Hubei Province, China. *Int. J. Environ. Res. Public. Health.* **19**, 178. https://doi.org/10.3390/ijerph19010178 (2022).

22. Li, Q., Pu, Y. C. & Zhang, Y. Study on the spatio-temporal evolution of land use in resource-based cities in three Northeastern provinces of China-an analysis based on long-term series. *Sustainability* **14**, 13683. https://doi.org/10.3390/SU142013683 (2020).

23. Yang, J. & Huang, X. The 30 m annual land cover datasets and its dynamics in China from 1985 to 2022 (Earth System Sci. Data) dataset. 1.0.2. https://doi.org/10.5281/zenodo.8176941 (2023).

24. Yu, Z., Li, M. Y., Qian, Y. Y., Peng, R. F. & Yang, G. X. Land use change and its ecological effects in three Gorges reservoir area based on CA-Markov model with multiple scenarios simulation. *Res. Soil. Water Conserv.* **31**, 363–372. https://doi.org/10.13869/j.cnki.rswc.2024.03.023 (2024).

25. Liu, S. Y., Zhang, Y. J., Xie, Y. Y., Zhang, Q. & Xi, H. C. Research on land use change in Huaihe river basin based on the CA-Markov model. *J. Irrig. Drain.* **43**, 52–59. https://doi.org/10.13522/j.cnki.ggps.2023309 (2023).

26. Liang, X. et al. Understanding the drivers of sustainable land expansion using a patch-generating land use simulation (PLUS) model: a case study in Wuhan, China. *Comput. Environ. Urban.* **85**, 101569. https://doi.org/10.1016/j.compenvurbsys.2020.101569 (2021).

27. Zhang, J. P., Wang, J., Chen, Y. H., Huang, S. D. & Liang, B. Y. Spatiotemporal variation and prediction of NPP in Beijing-Tianjin-Hebei region by coupling PLUS and CASA models. *Ecol. Inf.* **81**, 102620. https://doi.org/10.1016/J.ECOINF.2024.102620 (2024).

28. Zhi, J. J., Chu, C. Q., Han, C. X., Wang, X. T. & Zhang, L. K. Future construction land expansion under multiple simulation development scenarios and its impacts on landscape pattern evolution in China. *Geographical Res.* **43**, 843–860. https://doi.org/10.11821/dlyj020221191 (2024).

29. Liu, Y., Huang, T. T., Qiu, Z. Y., Guan, Z. L. & Ma, X. Y. Effects of precipitation changes on fractional vegetation cover in the Jinghe river basin from 1998 to 2019. *Ecol. Inf.* **80**, 102505. https://doi.org/10.1016/j.ecoinf.2024.102505 (2024).

30. Qiao, W. F. et al. Evaluation of intensive urban land use based on an artificial neural network model: a case study of Nanjing City, China. *Chin. Geogr. Sci.* **27**, 735–746. https://doi.org/10.1007/s11769-017-0905-7 (2017).

31. Jin, J., Wang, Z. H., Zhao, Y. P., Zhu, Z. J. & Zhang, J. Quantitative evaluation of the influence of rainfall changes and groundwater exploitation on the groundwater level: a case study of the Northern Huangqihai basin, China. *J. Water Clim. Change.* **14**, 1497–1514. https://doi.org/10.2166/wcc.2023.402 (2023).

32. Leo, B. *Random Forests Mach. Learn.* **45**, 5–32. https://doi.org/10.1023/A:1010933404324 (2001).

33. Li, F. H., Yang, W. J., Kang, D. K., Li, Z. Z. & Ma, H. Study on Spatial and Temporal evolution characteristics of surface water in arid area based on random forest algorithm. *Water Resour. Power.* **42**, 10–18. https://doi.org/10.20040/j.cnki.1000-7709.2024.2024114 6 (2024).

34. Ge, F., Xu, J. J. & Jia, F. M. Analysis of land use change and its driving factors in Foshan City from 2000 to 2020. *Nat. Resour. Informatization.* **6**, 66–72. https://doi.org/10.3969/j.issn.1674-3695.2023.06.011 (2023).

35. Musole, J., Hou, K. & Alan, R. X. J. Understanding land-use trade-off decision making using the analytical hierarchy process: insights from agricultural land managers in Zambia. *Land* 12, 532. (2023). https://doi.org/10.3390/land12030532

36. Wu, M. L. et al. Machine learning-based prediction of carbon fluxes in terrestrial ecosystems in China and its response to land use change. Preprint at. (2024). https://doi.org/10.13227/j.hjkx.202406133

37. Liu, J. Y. et al. A study on the spatial-temporal dynamic changes of land-use and driving forces analyses of China in the 1990s. *Geographical Res.* **22**, 1–12. https://doi.org/10.3321/j.issn:1000-0585.2003.01.0012003 (2003).

38. Inner Mongolia Autonomous Region People's Government. *Announcement of groundwater over-exploitation areas, prohibited exploitation areas and limited exploitation areas in Inner Mongolia Autonomous Region* (2015). https://www.nmg.gov.cn/zwgk/zfgb/2015n_4820/201503/201501/t20150112_301615. html.

39. Inner Mongolia Autonomous Region People's Government. *The 13th Five-Year Plan for ecological protection in Inner Mongolia Autonomous Region.* (2017). https://www.nmg.gov.cn/ztzl/sswghjh/lcgh/ssw/202012/t20201208_312916.html

40. People's Government of Ulanqab City. *Win the three major defensing battles to build an important ecological security barrier in Siziwwangqi Banner.* (2024). https://www.wulanchabu.gov.cn/qxdt/1374863.html

41. Today's Headlines. *Announcement on strengthening the implements on the Grass-Livestock Balance, Forbidden Grazing and Rest Grazing in 2024 in Siziwwangqi Banner.* (2024). https://www.toutiao.com/article/7352862890688365097/?upstream_biz=doubao&source=m_redirect

42. Inner Mongolia Autonomous Region People's Government. *Protection of farmland from multiple aspects: safeguarding the lifeline of grain production.* (2024). https://www.nmg.gov.cn/zwgk/zcjd/gjzcjd/202402/t20240209_2467611.html

43. Dong, Z. J. From land-use planning to territorial space planning: a perspective of scientific and rational planning. *China Land. Sci.* **34**, 1–7. https://doi.org/10.11994/zgtdkx.20200423.085446 (2022).

44. Xu, F. & Chi, G. Q. Spatiotemporal variations of land use intensity and its driving forces in China, 2000–2010. *Reg. Environ. Change.* **19**, 2583–2596. https://doi.org/10.1007/s10113-019-01574-9 (2019).

Acknowledgements

Author contributions

Jing Jin: Conceptualization, methodology, Funding acquisition, Writing-original draft, review & editing. Zilong Liao: Methodology, Formal analysis. Tiejun Liu: Conceptualization, Funding acquisition. Mingxin Wang: Investigation, Formal analysis; Jing Zhang: Investigation, Formal analysis. Xinjian Zhang: Data Curation, Formal analysis. Yining Fan: Data Curation.

Declarations

Competing interests

The authors declare no competing interests.

Additional information

Correspondence and requests for materials should be addressed to J.J.

Reprints and permissions information is available at www.nature.com/reprints.

Publisher's note Springer Nature remains neutral with regard to jurisdictional claims in published maps and institutional affiliations.